

## RESEARCH ARTICLE

# Iteratively Learning Reconstruction of Blade Tip-Timing Signals and Cointegration-Based Damage Detection Under Variable Conditions

ZHONGSHENG CHEN<sup>1,2</sup>, (Member, IEEE), HAOPENG LIU<sup>2</sup>, AND LIANYING LIAO<sup>1</sup>

<sup>1</sup>College of Automotive Engineering, Changzhou Institute of Technology, Changzhou 213032, China

<sup>2</sup>College of Electrical and Information Engineering, Hunan University of Technology, Zhuzhou 412007, China

Corresponding author: Zhongsheng Chen (chenzs@czu.cn)

This work was supported in part by the National Natural Science Foundation of China under Grant 51975206, in part by the Major Natural Science Foundation of the Higher Education Institutions of Jiangsu Province under Grant 22KJA460002, and in part by Changzhou Science and Technology Support Plan under Grant CE20225062.

**ABSTRACT** Blade tip-timing (BTT) is a direct blade vibration monitoring technique and how to use under-sampled BTT signals for blade damage detection is still challenging under variable conditions. Compressed sensing (CS) has been introduced for reconstructing BTT vibration signals, but classical CS reconstruction algorithms are limited by the sparsity and slow optimization process. In order to overcome this issue, this paper presents an iteratively learning reconstruction method by introducing the vector approximate message passing (VAMP) algorithm, called VampNet. Firstly, a discrete Multi-coset sampling (MCS)-based CS model is built for BTT vibration signals in order domain and an improved Hanning-Poisson window is integrated to reduce the order spectrum leakage in discretization. Then the VampNet model is proposed to reconstruct blade vibration engine orders (EOs) and the sensing matrix is discussed. Based on reconstructed vibration EOs, a cointegration-based method is proposed for blade damage detection, so that the influences of variable conditions can be reduced. Finally, the feasibility of the proposed method is testified by Matlab simulations and experimental dataset. The results show that blade vibration EOs can be accurately reconstructed by the VampNet and then small cracks can be detected by using the cointegrating residual.

**INDEX TERMS** Blade tip-timing, compressed sensing, learning reconstruction, damage detection, cointegration analysis.

## I. INTRODUCTION

Rotating blades are one kind of key components in the fields of new energy and aerospace. Different kinds of faults or damages are often caused in rotating blades due to high or low cycle fatigues. Accurate and on-line vibration monitoring of rotating blades is much necessary for safety. Up to now, some works on blade damage detection have been reported. Kaewniam et al. [1] reviewed the latest advances of damage detection in wind turbine blades, where signal processing techniques were classified into three groups:

The associate editor coordinating the review of this manuscript and approving it for publication was Zihuai Lin<sup>1</sup>.

time-domain analysis, frequency-domain analysis and time-frequency-domain analysis. Civera and Surace [2] proposed to use instantaneous spectral entropy and continuous wavelet transform for anomaly detection of wind turbines. Panagiotopoulos et al. [3] proposed time series-based damage detection of the blade under variable environmental and operating conditions. According to the literature, vibration analysis is an effective tool of online blade monitoring [4]. In most existing studies, accelerator sensors always have to be mounted on the nearby case of the blades due to the condition of continuous rotating. In this case, however, sampled vibration signal is a mixture of vibration signals from multiple components, rather than only blades. The consequence is that

it is not easy to detect weak blade damages due to signal contamination. Therefore, it is much significant to directly measure vibration signals of rotating blades.

In recent years, blade tip-timing (BTT) has been proved to be an advanced direct vibration monitoring method [5], [6]. Compared with using strain gauges [7], [8], the BTT method has the advantages of on-line, direct and non-intrusion measurement. Different from most existing studies in which vibration signals are sampled at the Nyquist sampling frequency, the BTT sampling frequency is equal to the product of the rotating speed and the number of BTT probes. In real-world applications, only few BTT probes can be admitted due to the space limitation and the cost. In this case, the BTT sampling frequency is too low to satisfy the Nyquist sampling theorem, leading to seriously under-sampled signals. Then it is hardly to directly capture ‘true’ blade vibration characteristics by using classical signal processing methods due to serious frequency alias. Therefore most existing damage detection methods cannot be used in the field of BTT and it is very necessary to achieve accurate reconstruction of BTT vibrations.

By now, BTT vibration reconstruction methods have been investigated in academia & industry. The whole development history can be divided into three stages. At the early stage, BTT vibration signal is considered as a narrow-band signal and its central frequency is assumed to be known in advance. In this case, Salhi et al. [9] first proposed to reconstruct continuous BTT vibration signals. Chen et al. [10] also presented a BTT vibration reconstruction method based on the Shannon theorem. In practice, however, blade vibrations tend to be multi-band due to system nonlinearity, aerodynamic excitations or potential damages. Chen et al. [11] presented a novel interpolation method for wideband BTT signal reconstruction. Cao et al. [12] developed an efficient time delay-based spectrum reconstruction method for BTT vibration signals. At the second stage, more attentions are paid on multi-band BTT vibration reconstruction based on sparse sensing. Lin et al. [13] proposed one novel method to reconstruct multi-mode BTT vibration signals based on sparse representation. Tian et al. [14] built a sparse reconstruction model of BTT vibration signals in the frequency domain. In particular, the compressed sensing (CS) theory proposed by Donoho [15] is an effective tool of analyzing sparse signals, which can be utilized to recover certain under-sampled signals. In recent years, the researchers began to introduce the CS theory for BTT vibration reconstruction. Xu et al. [16] first built a CS model of BTT vibration measurement and reconstructed the frequency spectrum of the blade by minimizing the norm. Pan et al. [17] used the dictionary learning method to represent BTT vibration signals and then reconstructed the frequency spectrum by using the basis pursuit algorithm. Spada and Nicoletti [18] discussed several necessary conditions of accurate BTT vibration reconstruction by applying the CS theory. Liu et al. [19] proposed conditions of BTT vibration reconstruction by using the MUSIC algorithm. In particular, multi-coset sampling (MCS)

is one special way of reducing the sampling rate of multi-band signals [20]. Chen et al. [21] first pointed out that BTT sampling was just a natural MCS scheme and then a MCS-based CS method was proposed under variable speeds. Classical CS reconstruction algorithms are mainly based on greedy algorithms and convex optimization methods. However, these algorithms have been restricted by the restriction of Restricted Isometry Property (i.e., the sparsity) and slow optimization process in practice. For this purpose, learning methods including deep learning (DL) are currently being introduced into the field of CS. Ye and Han [22] proposed a general DL framework for image reconstruction. Inspired by these studies, Chen et al. [23] proposed a deep compressed sensing (DCS) method for BTT vibration reconstruction by using convolutional neural network (CNN). But traditional deep neural networks (DNNs) have many layers for improving accuracy, leading to complex architectures. On the other hand, MCS-based CS can also be looked as one kind of linear sparse inverse problems. Fast iterative thresholding algorithms have been studied for these inverse problems as alternatives to convex optimization. Donoho et al. [24] proposed a new class of iterative thresholding algorithms for reconstructing sparse signals, namely the approximate message passing (AMP) algorithm. Low computational complexity of the AMP algorithm has made it an appealing alternative of solving linear inverse problems. Later, Rangan et al. [25] proposed the vector AMP (VAMP) algorithm to address the AMP’s fragility with respect to the sensing matrix. In order to introduce learning scheme to solve sparse linear inverse problems, Borgerding et al. [26] proposed a novel deep network by unfolding the VAMP algorithm, called the learned VAMP (LVAMP) network. Compared with classical DNNs, the outstanding features of the LVAMP network include simple architecture, few super-parameters and good interpretability. For this purpose, this paper will introduce the similar idea for BTT vibration reconstruction and damage detection. The flowchart is shown in Figure 1.

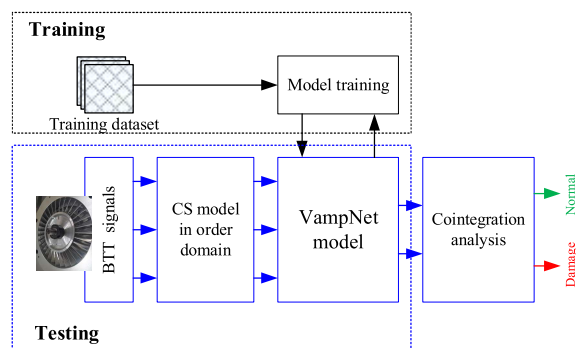


FIGURE 1. The flowchart of the proposed method in this paper.

The main contributions of this paper are threefold:

- i) A discrete-time CS model of BTT vibration signal is built in order domain, where the window function is applied to reduce the order spectrum leakage.

ii) A iteratively learning network is first introduced to reconstruct blade vibrations in order domain, called VampNet, which has the advantages of simple architecture, fewer super-parameters, and good interpretability.

iii) The cointegration analysis is carried out on reconstructed orders so that the effects of measurement noise and trend interrupt on damage detection can be eliminated greatly under variable operating conditions.

The remainder of this paper is summarized as follows. In Section II, the discrete MCS-based CS model of BTT vibration signals is built. Then the VampNet-based learning reconstruction model of BTT vibrations is derived in Section III and the reconstruction performance is discussed. In Section IV, cointegrating residual-based blade damage detection under variable conditions is proposed. Numerical simulations and experimental testing are done to validate the proposed method in Section V and Section VI, respectively. Finally, some conclusions are marked in Section VII.

## II. DISCRETE MCS-BASED CS MODEL OF BTT VIBRATION SIGNALS

### A. ANGULAR SAMPLING OF BTT VIBRATION SIGNALS

Basic process of the BTT method can be schematically represented as Figure 2. A bladed-disk with  $K$  blades and  $I$  BTT probes are embedded uniformly or non-uniformly into the stationary casing. At the same time, a once-per-revolution (OPR) sensor is placed in front of the rotating shaft, which is used as the timing reference by generating one pulse per revolution. Also it is assumed that the OPR sensor is on the same radius as the first BTT probe and the OPR marker is on the same radius as the first blade. Then the angles of the  $i^{th}$  ( $1 \leq i \leq I$ ) BTT probe and the  $k^{th}$  ( $1 \leq k \leq K$ ) blade relative to the OPR sensor are denoted as  $\alpha_i$  and  $\theta_k$ , respectively.

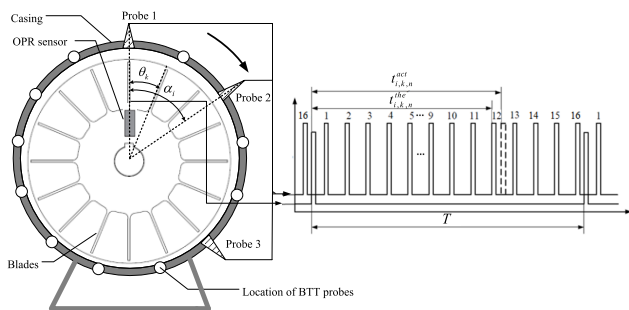


FIGURE 2. Schematic diagram of the BTT method.

According to the principle of the BTT method, the times of arrival (TOAs) are measured when each blade passes each BTT probe. Under no blade vibrations, theoretical TOAs of each blade are known in advance. However, once there are blade vibrations, the blades will pass BTT probes earlier or later than normal. In this case, actual TOAs will deviate from the theoretical TOAs, leading to time differences. Furthermore, these time differences are strongly related to blade vibration frequencies and amplitudes, so that blade vibrations

can be calculated. Classical BTT method is always carried out in time domain and the rotating speed is assumed to be fixed. However, the rotating speed is variable in real-world applications. In this case, the sampling time interval is not a constant, leading to unequally-sampled vibration signals. In particular, the vibration displacements cannot be calculated accurately.

As stated in [21], angular-domain sampling can be applied to overcome the issue of variable speeds. Interestingly, the BTT sampling process is just a natural angular-domain sampling pattern due to that all BTT probes are mounted circumferentially. ‘True’ angular-domain vibration displacement of the  $k$ th blade is denoted as  $y_k(\theta)$ , which is sampled for  $I$  times during each revolution according to Figure 1. The ideal sampling function of the  $i$ th BTT probe can be represented as,

$$p_k^i(\theta) = \begin{cases} \sum_{n=-\infty}^{+\infty} \delta[\theta - (2\pi n + \alpha_i - \theta_k)], \\ (n = 0, 1, 2, \dots), \theta_k \leq \alpha_i \\ \sum_{n=-\infty}^{+\infty} \delta[\theta - (2\pi n + 2\pi + \alpha_i - \theta_k)], \\ (n = 0, 1, 2, \dots), \theta_k > \alpha_i \end{cases} \quad (1)$$

where  $\delta$  is the Dirac delta function. Then the sampled vibration displacement of the  $k$ th blade in angular domain can be calculated as

$$\hat{y}_k(\theta) = \sum_{i=0}^{j-1} \sum_{n=-\infty}^{+\infty} y_k(\theta) \delta[\theta - (2\pi n + 2\pi + \alpha_i - \theta_k)] + \sum_{i=j}^{I-1} \sum_{n=-\infty}^{+\infty} y_k(\theta) \delta[\theta - (2\pi n + \alpha_i - \theta_k)] \quad (2)$$

where  $j = \{j | \alpha_{j-1} \leq \theta_k \leq \alpha_j\}$ .

### B. DISCRETE CS OF BTT VIBRATION SIGNALS IN ORDER DOMAIN

The sampling scheme in Equation (2) can be looked as  $I$ -channel parallel sampling with fixed angle delays. Furthermore, such a sampling pattern is equivalent to a MCS framework. Then the MCS can be used to represent the BTT vibration signals. Similar to time-domain signals, sampled BTT vibration signals are not sparse in angular domain, but sparse in order domain, so the MCS-based CS can be utilized here.

According to the MCS principle, it is assumed that  $L$  virtual BTT probes are uniformly mounted in the casing around the bladed-disk and the number of each probe is set from 1 to  $L$  clockwise. Here  $L$  should be selected to satisfy the Nyquist sampling theorem, so that real vibration engine orders (EOs) can be obtained. In practice,  $I$  actual BTT probes in Figure 1 are chosen from the above  $L$  virtual BTT probes, which is called as a MCS pattern  $(L, I, C)$ , where  $C = \{c_i : 1 \leq i \leq I\}$ ,  $c_i$  is the number of the  $i$ th BTT probe in the  $L$  probes ( $0 \leq c_1 < c_2 < \dots < c_I \leq L - 1$ ). For a given blade, the sampled vibration signals by all  $L$  probes and the

$i$ th BTT probe are denoted as  $y(\theta)$  and  $\bar{y}_i(\theta)$ , respectively. Furthermore, the relationship between  $\bar{y}_i(\theta)$  and  $y(\theta)$  can be derived as [21],

$$\bar{\mathbf{Y}}(O) = \Phi \tilde{\mathbf{Y}}(O) \quad (3)$$

where,

$$\bar{\mathbf{Y}}(O) = [L\bar{Y}_1(O) \exp(-j2\pi Oc_1), \dots, L\bar{Y}_I(O) \exp(-j2\pi Oc_I)]^T,$$

$$\tilde{\mathbf{Y}}(O) = [Y_1(O), \dots, Y_L(O)]^T,$$

$$\Phi_{I \times L} = \begin{bmatrix} \exp[j2\pi c_1 \times 0/L] \cdots \exp[j2\pi c_1 (L-1)/L] \\ \vdots \quad \ddots \quad \vdots \\ \exp[j2\pi c_I \times 0/L] \cdots \exp[j2\pi c_I (L-1)/L] \end{bmatrix},$$

$$Y_k(O) = Y \left( O_0 - \left( k - \frac{L+1}{2} \right) / L \right),$$

$$k = 1, 2, \dots, L, \quad O_0 \in [-1/2, 1/2],$$

$Y(O)$  and  $\bar{Y}_i(O)$  are the DFTs of  $y(\theta)$  and  $\bar{y}_i(\theta)$ , respectively.

It can be seen that  $Y(O)$  is equally divided into  $L$  sub-bands and  $Y_k(O)$  is the  $k$ th sub-band. According to Equation (3),  $\bar{Y}_i(O)$  can be looked as the weighed sum of all sub-bands of  $Y(O)$ . In real-world applications,  $\bar{\mathbf{Y}}(O)$  can be calculated by  $I$  actual BTT measurements and  $\Phi$  depends on the MCS pattern. Then the reconstruction task is to recover the unknown  $\tilde{\mathbf{Y}}(O)$  based on  $\bar{\mathbf{Y}}(O)$  and  $\Phi$ , so that the expected  $Y(O)$  can be obtained. Furthermore,  $\tilde{\mathbf{Y}}(O)$  is sparse due to that it only has few non-zero rows. Thus Equation (3) is equivalent to a CS problem. On the other hand, the order in Equation (3) is continuous so that discrete DFT should be done. The discretization process can be simplified as the following steps.

i) Taking a sampling sequence with  $M$  (a power of two) samples from each BTT probe and calculating  $M$ -point discrete DFT. The discrete DFT of the sampling sequence of the  $i$ th BTT probe is calculated as,

$$\bar{Y}_i[k] = \sum_{n=0}^{M-1} y_i[n] \exp(-j2\pi nk/M), \quad k = 0, \dots, M-1 \quad (4)$$

ii) Calculating  $\bar{\mathbf{Y}}$ .

$$\bar{\mathbf{Y}}_{I \times M} = L \times \begin{bmatrix} \bar{Y}_1[1] e^{-j2\pi c_1 \times 0/LM} \cdots \bar{Y}_1[M] e^{-j2\pi c_1 \times (L-1)/LM} \\ \vdots \quad \ddots \quad \vdots \\ \bar{Y}_I[1] e^{-j2\pi c_I \times 0/LM} \cdots \bar{Y}_I[M] e^{-j2\pi c_I \times (L-1)/LM} \end{bmatrix} \quad (5)$$

iii) Rewriting Equation (3) as the following discrete model.

$$\bar{\mathbf{Y}}_{I \times M} = \Phi_{I \times L} \tilde{\mathbf{Y}}_{L \times M} \quad (6)$$

iv) Reconstructing  $\tilde{\mathbf{Y}}(O)$  by the learning model and then re-arranging  $\tilde{\mathbf{Y}}(O)$  to obtain  $Y(O)$ . Discrete  $\tilde{\mathbf{Y}}(O)$  is a  $L \times M$  matrix, which can be re-arranged to a  $1 \times LM$  vector by connecting successively all rows of  $\tilde{\mathbf{Y}}(O)$ , leading to the discrete order spectrum ( $Y(O)$ ).

### III. VAMPNET-BASED LEARNING RECONSTRUCTION METHOD OF BTT VIBRATION SIGNALS

#### A. VAMPNET-BASED LEARNING RECONSTRUCTION MODEL

As for the reconstruction problem in Equation (6), iterative thresholding algorithms are more efficient than classical CS reconstruction algorithms [24]. Furthermore, the VAMP algorithm is just one kind of iterative thresholding algorithms with low-complexity [25]. As shown in Figure 3, the VAMP algorithm is composed of two stages, namely minimum mean square error (MMSE) estimation and shrinkage stages. Each stage is comprised of four steps: estimation, divergence computation, Onsager correction and variance computation. The ‘‘Onsager correction’’ operation is used to decouple the iteration errors.

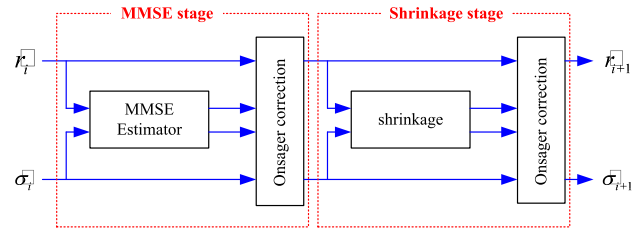


FIGURE 3. Schematic diagram of the VAMP algorithm.

Recently, learning reconstruction is introduced to reduce the constraint of sparsity in CS problems. Inspired by this idea, Borgerding et al. [26] proposed the learned VAMP network, where the iterative process was unfolded to a deep network. By referring to it, the VampNet is proposed for learning reconstruction of BTT vibration signals in this paper. By unfolding the process of the VAMP algorithm to  $P$  iterations, a  $P$ -layer VampNet is built as Figure 4.

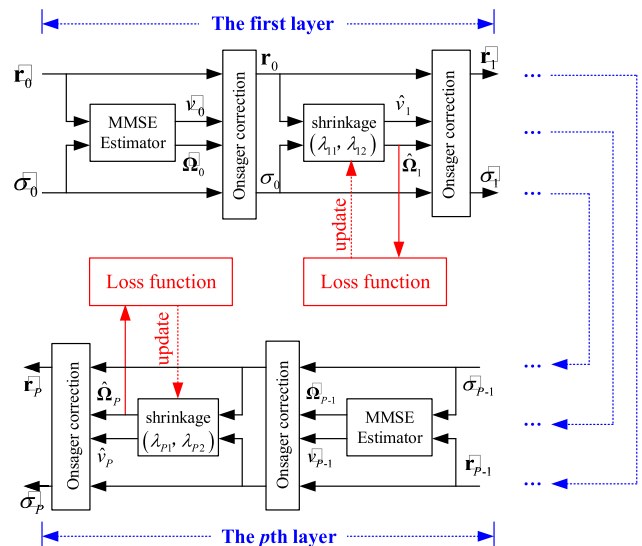


FIGURE 4. Schematic structure of the VampNet model.

Different from sparse linear inverse problems in most existing references, all matrixes in Equation (6) are complex.

In order to using the VampNet, firstly Equation (4) is converted into the following real-value form.

$$\Psi = \mathbf{A}\Omega \quad (7)$$

where,

$$\Psi_{2I \times M} = \begin{bmatrix} \text{Re}(\tilde{\mathbf{Y}}) \\ \text{Im}(\tilde{\mathbf{Y}}) \end{bmatrix}, \mathbf{A}_{2I \times 2L} = \begin{bmatrix} \text{Re}(\Phi) & -\text{Im}(\Phi) \\ \text{Im}(\Phi) & \text{Re}(\Phi) \end{bmatrix},$$

$$\Omega_{2L \times M} = \begin{bmatrix} \text{Re}(\tilde{\mathbf{Y}}) \\ \text{Im}(\tilde{\mathbf{Y}}) \end{bmatrix},$$

$\text{Im}(\cdot)$  denotes the imaginary part and  $\text{Re}(\cdot)$  denotes the real part.

In Figure 3, the  $i$ th layer has only several parameters to be learned, which depends on the shrinkage function.  $\hat{\Omega}_i$  in the  $i$ th layer is the approximation of  $\Omega$  and  $\hat{\Omega}_P$  in the  $P$ th layer is the final reconstruction of  $\Omega$ .

For the VAMP algorithm, the sensing matrix  $\mathbf{A}$  should be right-rotationally invariant, which is difficult to satisfy in practice. For this purpose, the singular value decomposition (SVD) of  $\mathbf{A}$  is often applied, i.e.,

$$\mathbf{A} = \mathbf{U}\mathbf{S}\mathbf{V}^T \quad (8)$$

Similar to classical DL methods, the VampNet training process is also composed of forward and backward operations.

Forward operation: The output of the  $i$ th layer is the input of the  $(i + 1)$ -th-layer. In the  $i$ th layer, the estimations at the MMSE stage can be summarized as, [26]

$$\tilde{\Omega}_{i-1} = \mathbf{v} \left( \mathbf{S}^2 + \frac{\sigma_w^2}{\tilde{\sigma}_{i-1}^2} \mathbf{I} \right)^{-1} \left( \mathbf{S}\mathbf{U}^T \Psi + \frac{\sigma_w^2}{\tilde{\sigma}_{i-1}^2} \mathbf{v}^T \tilde{\mathbf{r}}_{i-1} \right) \quad (9)$$

$$\tilde{v}_{i-1} = \frac{1}{N} \sum_{j=1}^R \frac{1}{s_j^2 \tilde{\sigma}_{i-1}^2 / \sigma_w^2 + 1} \quad (10)$$

$$\tilde{\mathbf{r}}_{i-1} = \frac{\tilde{\Omega}_{i-1} - \tilde{v}_{i-1} \tilde{\mathbf{r}}_{i-1}}{1 - \tilde{v}_{i-1}} \quad (11)$$

$$\sigma_{i-1}^2 = \frac{\tilde{\sigma}_{i-1}^2 \tilde{v}_{i-1}}{1 - \tilde{v}_{i-1}} \quad (12)$$

where  $\sigma_w^2$  is the variance of the stochastic noise,  $R = \text{rank}(\mathbf{A})$  and  $s_i$  denotes the  $i$ th singular value of  $\mathbf{A}$ .

The shrinkage stage is strongly related to the choice of the shrinkage function, which includes several learnable parameters. According to [26], here a zero-mean Bernoulli-Gaussian function with two parameters  $\lambda_i = [\lambda_{i1}, \lambda_{i2}]$  is selected as the shrinkage function. In this case, the estimations at the shrinkage stage can be summarized as,

$$\hat{\Omega}_i = \frac{\tilde{\mathbf{r}}_{i-1}}{\left( 1 + \frac{\sigma_{i-1}^2}{\lambda_{i1}} \right) \left( 1 + \sqrt{1 + \frac{\lambda_{i1}}{\sigma_{i-1}^2}} \exp \left[ \lambda_{i2} - \frac{\mathbf{r}_{i-1}^2}{2\sigma_{i-1}^2(1 + \sigma_{i-1}^2/\lambda_{i1})} \right] \right)} \quad (13)$$

$$\hat{v}_i = \left\langle \frac{\partial \hat{\Omega}_i}{\partial \mathbf{r}_{i-1}} \right\rangle \quad (14)$$

$$\tilde{\mathbf{r}}_i = \frac{\hat{\Omega}_i - \hat{v}_i \mathbf{r}_{i-1}}{1 - \hat{v}_i} \quad (15)$$

$$\tilde{\sigma}_i^2 = \frac{\sigma_{i-1}^2 \hat{v}_i}{1 - \hat{v}_i} \quad (16)$$

where  $\langle \cdot \rangle$  denotes the mean operation.

Backward updating: the parameters of  $\{\lambda_1, \dots, \lambda_P\}$  need to be learned by using training datasets  $\{(\Psi, \Omega)\}$ . Similar to classical DL methods the back-propagation algorithm driven by an optimizer is used to update the parameters. Differently, each layer of the VampNet has a local loss function. In this paper, the commonly used loss function (i.e. mean squared error) is adopted as follows.

$$L_i(\lambda_i) = \frac{1}{N} \sum_{k=1}^N \left\| \hat{\Omega}_i(\Psi^{(k)}; \lambda_i) - \Omega^{(k)} \right\|_2 \quad (17)$$

where  $N$  is the batch size and  $\|\cdot\|_2$  denotes the 2-norm operator. At the same time, the initial inputs of the VampNet are determined as:  $\tilde{\mathbf{r}}_0$  is generated randomly and

$$\tilde{\sigma}_0^2 = \left\| \Psi^{(k)} \right\|_2^2 / N \quad (18)$$

After training, the  $P$ -layer VampNet can be used to reconstruct the order spectrum of a blade based on  $I$ -channel BTT vibration signals.

Furthermore, the advantages of the VampNet can be summarized as: i) The VampNet has few layers ( $P$ ) and super-parameters ( $2P$ ), so its architecture is very simple; ii) Estimations at both the MMSE and shrinkage stages are based on simple math operations, so its computation complexity is much low; iii) The output ( $\hat{\Omega}_i$ ) of each layer is the approximation of  $\Omega$  (expected order spectrum), so the training process is much explainable, rather than a black-box learning framework in classical DNNs.

## B. PERFORMANCE ANALYSIS OF VAMPNET-BASED BTT VIBRATION RECONSTRUCTION

Reconstruction performance is the key point in engineering applications. As for the proposed VampNet, the influencing factors can be divided into three main categories. The first class is the MCS pattern, including the number of the BTT probes and the configuration of the  $I$  BTT probes (e.g. the sensing matrix). The second class is the VampNet architecture, including the number of layers, the shrinkage function, the optimizer and the loss function. The third class is the discretization of the MCS-based CS model. This paper will only focus on the MCS pattern and the discretization process.

### 1) DISCUSSION ON THE MCS PATTERN

According to the principle of the VAMP algorithm, the sensing matrix  $\mathbf{A}$  should be a right-rotationally invariant matrix. Furthermore, the SVD error can be utilized to evaluate how much  $\mathbf{A}$  is close to be right-rotationally invariant, which is

defined as,

$$\|\Delta \mathbf{A}\|_2 = \left| 20 \lg \left[ \left\| \mathbf{A} - \bar{\mathbf{U}}\sqrt{\Sigma} \left( \mathbf{A}^T \bar{\mathbf{U}}/\sqrt{\Sigma} \right)^T \right\|_2 / \|\mathbf{A}\|_2 \right] \right|, \quad \text{with } \mathbf{A}\mathbf{A}^T = \bar{\mathbf{U}}\Sigma\bar{\mathbf{V}}^T \quad (19)$$

Therefore, once  $I$  is determined,  $C$  needs be selected to obtain the minimum  $\|\Delta \mathbf{A}\|_2$ . Furthermore, the sensing matrix  $\mathbf{A}$  also depends on the  $C$ , so  $\mathbf{A}$  can be determined according to the following rule.

$$\mathbf{A} \propto \left\{ C \left| \min_{C, I} \|\Delta \mathbf{A}\|_2 \right. \right\} \quad (20)$$

## 2) DISCUSSION ON THE DISCRETIZATION PROCESS

Discretization brings undesirable feature of spectrum leakage to  $\bar{\mathbf{Y}}_{I \times M}$  and  $\mathbf{Y}_{L \times M}$  in Equation (6) and Equation (7). In this case, big error will be induced into the CS model of Equation (7). To deal with it, windowing is an effective solution. Instead of using traditional window functions, an improved Hanning-Possion (IHP) window is introduced to reduce spectrum leakage, which is defined as follows [27].

$$w_{(a,b)}[n] = (1 - 2|n|/K)^a e^{-b(2|n|/K)^2}, \quad n \in [-K/2, K/2 - 1] \quad (21)$$

where  $a$  and  $b$  are two controllable parameters,  $K$  is the window length.

The unique feature of the IHP window is that the sidelobes can be controlled by  $a$  and  $b$ . In particular, there is almost no sidelobes when  $b$  is optimal. Then the IPH window can be integrated into Equation (4).

In the end, the relative root mean square (RRMS) is defined to evaluate the reconstruction performance as follows.

$$\text{RRMS} = 10 \log \sqrt{\frac{\sum_{i=1}^{LM} (\hat{y}[i] - y[i])^2}{\sum_{i=1}^{LM} y^2[i]}} \quad (22)$$

where  $y[i]$  and  $\hat{y}[i]$  are the original and reconstructed order spectrum of BTT vibration signals, respectively.

## IV. COINTEGRATION-BASED BLADE DAMAGE DETECTION UNDER VARIABLE OPERATION CONDITIONS

Up to now, many blade damage detection methods have been studied in the literature, including time-domain, frequency-domain and time-frequency-domain methods. However, these methods are often based on Nyquist sampled signals, so they cannot be directly utilized in the field of BTT. Even though vibration reconstruction methods can be applied, it is almost impossible to obtain accurate time-domain signals. Under constant rotating speeds, the authors proposed a crack detection method based on time-domain and frequency-domain features [10]. Under variable speeds, however, it is very difficult to obtain these features. To our best knowledge, it is first to study BTT-based damage detection under variable conditions. It has to face big challenges. For example, environmental temperature often changes under variable

operation conditions, which has obvious effect on blade natural frequencies. In order to remove the influences of environmental variations on damage detection, cointegration analysis is a promising method. The concept of cointegration was proposed in 1987, which was a technique used to find a possible correlation among time series processes in the long term [28]. Several non-stationary variables can be cointegrated if some linear combination of them is stationary, so that the common trends caused by the environmental and operational conditions can be removed. Cross et al. [29] studied the cointegration procedure for structural health monitoring. In this paper, the cointegration is introduced for blade damage detection and the detailed steps are summarized as Figure 5.

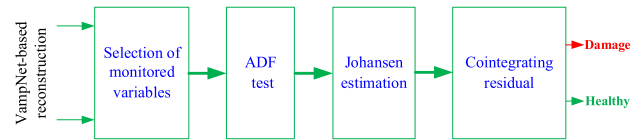


FIGURE 5. Schematic process of cointegration-based blade damage detection.

1) Selection of monitored variables. After VampNet-based reconstruction, discrete order spectrum of the blade can be written as an  $LM$ -dimensional vector ( $\mathbf{Y} = [Y[0], Y[1], \dots, Y[i], \dots, Y[LM - 1]]^T$ ), where each element is considered as a candidate monitored variable. As for blade damage detection,  $Q$  monitored variables are selected from  $\mathbf{Y}$  according to the prior knowledge, namely the amplitudes of the order spectrum at integer and fractional orders. At the same time, each monitored variable should have the same integrated order. Then the  $Q$  monitored variables are denoted as  $\mathbf{X} = [x_1, \dots, x_Q]^T$ ,  $x_i \in \{Y[0], \dots, Y[LM - 1]\}$ . By using  $N$  observations, a  $Q$ -dimensional multivariate time series can be obtained as follows.

$$\mathbf{X} = \begin{bmatrix} x_1[1] & \cdots & x_1[N] \\ \vdots & \ddots & \vdots \\ x_Q[1] & \cdots & x_Q[N] \end{bmatrix} \quad (23)$$

2) The augmented Dickey-Fuller (ADF) test.

In practice, the integrated order is always equal to 1 or 2 due to that time series is generally not divergent. In this paper, each monitored variable is considered as integrated order one  $I(1)$ . In order to ascertain the integration order of each time series ( $\mathbf{x}_i = \{x_i[1], \dots, x_i[N]\}$ ), the augmented Dickey-Fuller (ADF) test will be applied, which is based on a unit root test for each time-series.

3) The Johansen estimation.

There are two common methods to find the cointegrating vector, namely the Engle-Granger two-step estimation and the Johansen estimation. In this paper, the Johansen estimation procedure is adopted, which is based on the maximum-likelihood multivariate estimation. When the monitored variables are cointegrated, the cointegrating vector

( $\Psi = [\psi_1, \dots, \psi_Q]^T$ ) can be estimated by the Johansen procedure. Then the cointegrating residual of the  $i$ th observations can be estimated as

$$r_i = \sum_{j=1}^Q \psi_j x_j [i] \quad (24)$$

4) Cointegrating residual-based damage detection.

In order to perform blade damage detection, the cointegrating vector of normal samples is calculated and the cointegrating residual can be obtained. Then the upper and lower bounds of the cointegrating residual under normal conditions are defined as  $r_{base}^U = \bar{r} + 3\sigma$  and  $r_{base}^L = \bar{r} - 3\sigma$  respectively, where  $\bar{r}$ ,  $\sigma$  are the mean and derivation of the cointegrating residual sequence. In engineering applications, the cointegrating residual is continually monitored during operations. If the cointegrating residual significantly deviates from the interval defined as  $[r_{base}^L, r_{base}^U]$ , it indicates the occurrence of some damage in the blade.

V. NUMERICAL VALIDATION AND DISCUSSIONS

A. SIMULINK-BASED DATASET PREPARATION

The angular-domain BTT sampling process can be simulated by Matlab/Simulink and the whole model is composed of the dynamic model and angular-domain sampling module [23]. For the sake of simplicity, dynamic behavior of one blade can be represented by the following single-degree-of-freedom (SDOF) lumped-parameter model.

$$m_{eq}\ddot{y}(t) + c_{eq}\dot{y}(t) + k_{eq}y(t) = F(t) \quad (25)$$

where  $m_{eq}$ ,  $c_{eq}$ ,  $k_{eq}$  denotes the equivalent mass, damping and stiffness, respectively.  $y(t)$  denotes blade vibration displacement.  $F(t)$  denotes vibration excitation.

Furthermore,  $k_{eq}$  can be looked as a constant ( $k_{eq} = k_{eq}^n$ ) when the blade is healthy. On the other hand, when there is a crack in the blade, the crack is always in the ‘breathing’ state. In this case,  $k_{eq}$  will be time varying with the vibration excitation. In this paper, the harmonic excitation is defined as

$$F(t) = \sum_{j=1}^J A_j \sin(E_j \theta(t) + \varphi_j)$$

$$\theta(t) = 2\pi \int_0^t f_r(t) dt, f_r(t) = f_0 + (f_e - f_0)t/T_s \quad (26)$$

where  $E_j$  denotes the vibration order,  $J$  is the number of vibration orders,  $A_j$  is the excitation amplitude,  $\varphi_j$  denotes the phase,  $f_r(t)$  denotes the variable rotating speed,  $f_0, f_e$  are the rotating frequencies at the starting time and the ending time respectively,  $T_s$  is the total simulation time,  $\varphi_j$  denotes the phase.

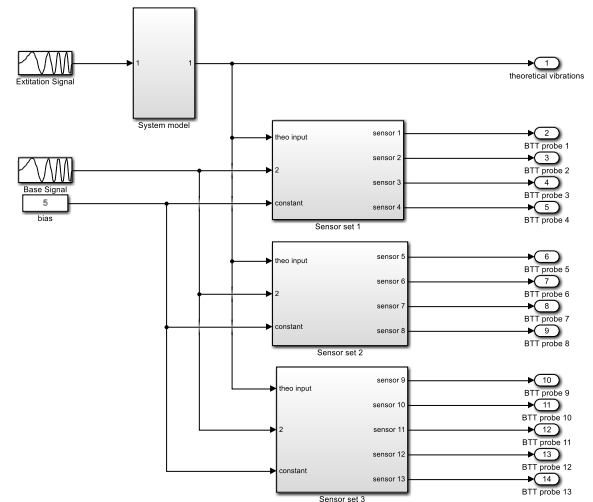
Then the time-varying equivalent stiffness can be represented as [30],

$$k_{eq}^c(t) = k_{eq}^{open} + \frac{1}{2} \left( 1 + \sum_{j=1}^J A_j \sin(E_j \theta(t) + \varphi_j) \right)$$

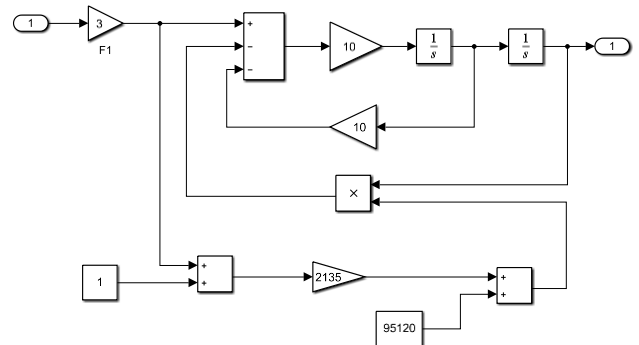
$$\times (k_{eq}^{close} - k_{eq}^{open}) \quad (27)$$

where  $k_{eq}^{open}$  denotes the equivalent stiffness when the crack is fully open,  $k_{eq}^{close}$  denotes the equivalent stiffness when the crack is fully closed (eg.  $k_{eq}^{close} = k_{eq}^n$ ).

In this simulation, only one vibration order is considered, i.e.  $J=1$ . Healthy and cracked blades can be simulated by using the corresponding equivalent stiffness in the Matlab/Simulink model, respectively. Angular-domain BTT sampling process for cracked blade is built as Figure 6 and the simulation parameters are listed in Table 1. Then BTT vibration signals of healthy and cracked blade are recorded respectively. Finally, the dataset composed of  $\Psi$ ,  $\mathbf{A}$  and  $\Omega$  can be used to prepare training and testing samples for the VampNet. After trials, a 4-layer VampNet is built and the optimizer of ‘Gradient Descent’ with a learning rate 0.001 is utilized.



(a) The whole simulation model



(b) Details of the ‘System model’ module

FIGURE 6. Simulink model of angular-domain BTT sampling process for cracked blade.

B. COMPARISON OF DIFFERENT WINDOW FUNCTIONS

As stated before, Equation (3) always holds in theory. But for training and testing samples,  $\Psi$ ,  $\mathbf{A}$  and  $\Omega$  are generated

TABLE 1. Values of simulation parameters.

| Parameters                     | Values   |
|--------------------------------|--|
| $\{m_{eq}, c_{eq}, k_{eq}^n\}$ | $\{0.1 \text{ kg}, 10 \text{ N} \cdot \text{s} / \text{m}, 99390 \text{ N} / \text{m}\}$ |
| $\{f_0, f_e\}$                 | $\{20 \text{ Hz}, 100 \text{ Hz}\}$  |
| $k_{eq}^{open}$                | 95120 N/m  |
| $k_{eq}^{close}$               | 99390 N/m  |
| $T_s$                          | 50 s   |
| $E_1$                          | 2  |
| $A_1$                          | 3  |
| $L$                            | 13   |
| $\varphi_1$                    | 0  |
| Optimizer                      | GradientDescent  |
| Learning rate                  | 0.001  |

by discrete DFT of sampled BTT vibration signals. Due to the order spectrum leakage in discretization,  $\Psi$  is not exactly equal to  $\mathbf{A}\Omega$ , leading to the discretization error which is defined as,

$$\Delta \mathbf{d} = \Psi - \mathbf{A}\Omega \quad (28)$$

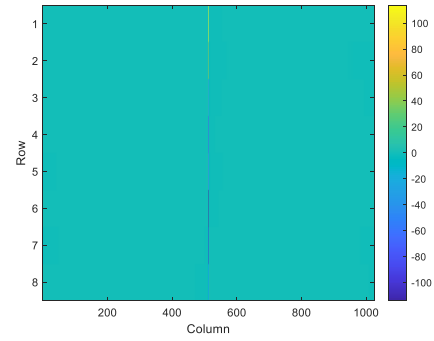
where  $\Delta \mathbf{d}$  is the error matrix with the dimension of  $L \times M$ . Obviously, the smaller the discretization error, the closer  $\Delta \mathbf{d}$  is to the zero matrix.

Next, three window functions are applied to reduce the discretization error respectively: the rectangular window, the Hanning window and the IHP window with  $a = 1 \times 10^{-4}$ ,  $b = 20$ . Four BTT probes are selected and 1024-point discrete DFT is done. The results under using three window functions are shown and compared in Figure 7. It can be seen that components in Figure 7 (c) are much closer to zero than those in Figure 7 (a) and (b), which indicates that using the IHP window is the best to reduce the discretization error.

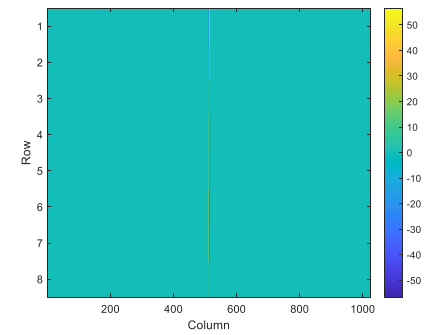
### C. INFLUENCES OF KEY FACTORS ON THE RECONSTRUCTION PROCESS

Firstly,  $C$  in the MCS pattern is an important influencing factor of vibration reconstruction. Therefore, it is necessary to investigate the effect of  $C$ . The number of BTT probes is selected as 4. According to Equation (18), the best  $C$  ( $C = (1, 2, 5, 7)$ ) and the worst  $C$  ( $C = (3, 6, 9, 12)$ ) are selected. Then the 4-layer VampNet is trained by using the training samples under each  $C$ , respectively. Here no other windows (e.g. using rectangular window) are applied in the DFT. After 300 iterations, the reconstruction RRMSs of all layers are plotted and compared in Figure 8. It can be seen that the RRMSs of the second, the third and the fourth layers under  $C = (1, 2, 5, 7)$  is much less than those under  $C = (3, 6, 9, 12)$ . Therefore, selecting proper MCS pattern is much necessary in real-world applications.

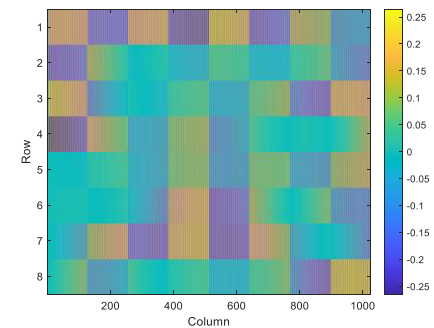
Secondly, the window function is another important influencing factor of reconstruction. Here, the rectangular window, the Hanning window and the IHP window are con-



(a) Rectangular window



(b) Hanning window



(c) IHP window

FIGURE 7. Comparison of the discretization errors using three different window functions.

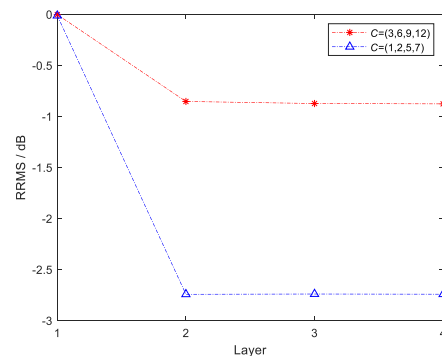


FIGURE 8. Comparison of RRMS under two MCS patterns.

sidered, respectively. Then the 4-layer VampNet is trained by using the training samples under  $C = (1, 2, 5, 7)$ . After 300 iterations, the reconstruction RRMSs of all layers using



the three windows are plotted and compared in Figure 9. It can be seen that using the proposed IHP window lead to the least RRMS and using the rectangular window lead to the maximum RRMS. Furthermore, their training processes of each layer are plotted in Figure 10. As for the output layer, the iteration number using the IHP window is less than that using the rectangular window. The results testify the superiority of the proposed IHP window again. At the same time, the original and reconstructed order spectra are compared in Figure 11, which shows that the proposed VampNet-based reconstruction method is much effective. It should be pointed out that the whole range of reconstructed order spectrum is  $[-13/2, 13/2]$ , so the negative side is shown. In practice, negative orders are meaningless.

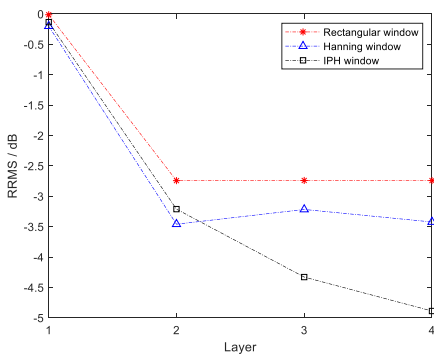


FIGURE 9. Comparison of RRMS under using three windows.

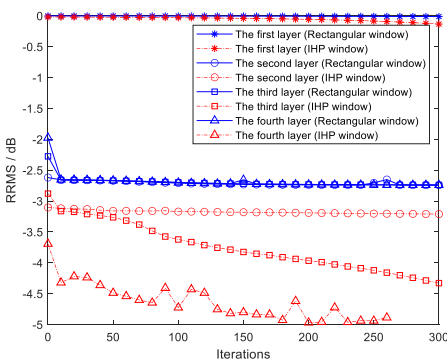


FIGURE 10. Training process using two different windows.

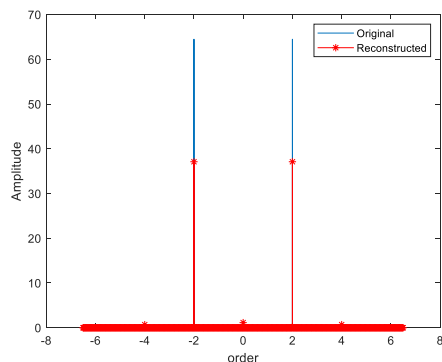


FIGURE 11. Reconstructed results.

TABLE 2. Comparison with CNN-based reconstruction methods.

| Metrics          | CNN-like models | VampNet model |
|------------------|-----------------|---------------|
| Architecture     | Complex         | Simple        |
| Super-parameters | Many            | Few           |
| Loss function    | Global          | Local         |
| Training dataset | Needed          | Needed        |
| Interpretability | Poor            | Good          |
| Inference speed  | Moderate        | Fast          |

Finally, in the previous work [23], the authors also investigated CNN-based method of BTT vibration reconstruction. The results indicated that the CNN model could also achieve accurate reconstruction after training. From the viewpoint of BTT vibration reconstruction, the VampNet model and CNN-like modes are compared in Table 2. It can be seen that the VampNet model is more suitable for engineering application than CNN-like modes. In addition, Ye et al. [22] also revealed the limitations of many existing DNNs for CS problems.

#### D. DCOINTEGRATION-BASED BREATHING CRACK DETECTION

According to Figure 5, firstly it needs to select candidate monitored variables. Based on the prior knowledge [30], Super-harmonic/sub-harmonic vibrations will be caused by damages. Therefore, the amplitudes at the first, third, fourth and fifth orders in the reconstructed order spectra are determined as the candidate monitored variables. Then the Matlab/Simulink model in Section V-A is used to chronologically generate 1000 groups of normal samples and crack samples, respectively. The length of each group is 1024.

Firstly, the proposed VampNet model is used to reconstruct the order spectra of each normal & crack sample and the monitored variables are calculated. In this way, time series of each monitored variable can be built. In order to simulate the trend term, the same stochastic signal varying linearly with time is added to the above each time series. Simulated time series of all monitored variable from normal samples are shown in Figure 12. Next, the ADF test is carried out on the simulated time series and the cointegrating vector is estimated as  $[2.5597, -1.1643, -2.6146, 3.3329]$  by using the Johansen estimation.

Secondly, the estimated cointegrating vector is used to calculate the cointegrating residual of the normal samples and the result is shown in Figure 13. It can be seen that the cointegrating residual is almost a stationary time series with zero mean, so that the trend term is obviously eliminated. Furthermore, the cointegrating residual of the crack samples is estimated and the result is shown in Figure 14. It can be seen that the cointegrating residual of the crack samples greatly deviates from that of the normal samples. Thus the simulation results show that the cointegrating residual-based method can be applied to accurately detect the blade's damage.

In addition, the effect of noise on the damage detection method is also studied. The results under two different

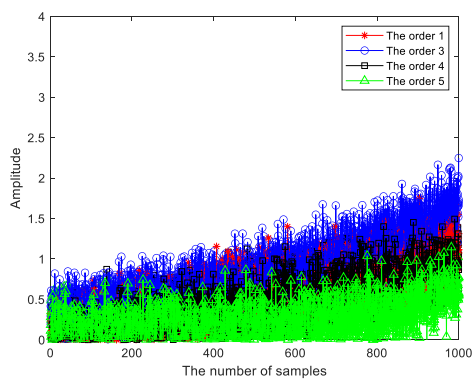


FIGURE 12. Reconstructed monitored variables.

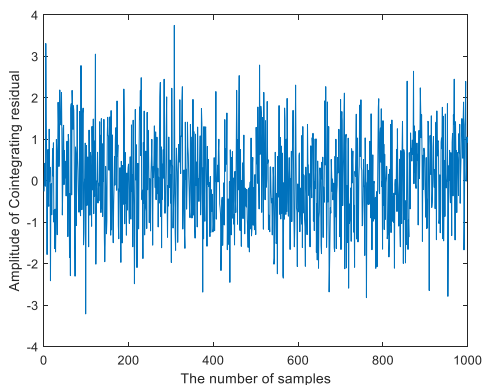


FIGURE 13. Cointegrating residual of normal samples.

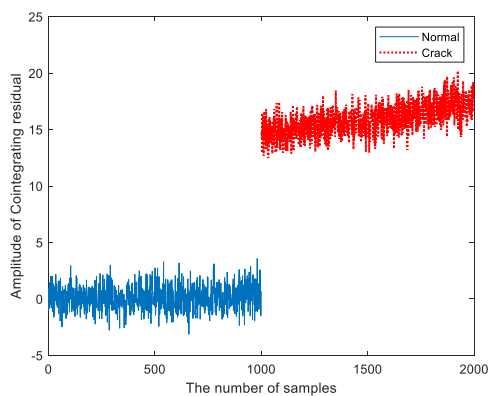


FIGURE 14. Cointegrating residual-based crack detection.

signal-to-noise ratios (SNRs) are shown in Figure 15. It can be seen that: i) Blade crack can still be effectively detected based on the cointegrating residual when noises exist; ii) Noises can reduce the damage detection capability.

### VI. EXPERIMENTAL VALIDATIONS

In order to further testify the proposed method, an experimental set-up of BTT-based vibration monitoring is shown in Figure 16(a). The whole experimental system is composed of a supporting base, an electrical motor, a testing bladed disk

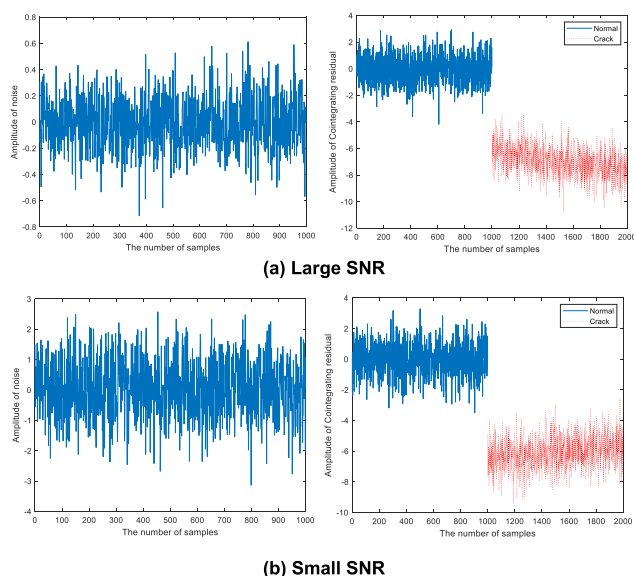


FIGURE 15. Crack detection under (a) large and (b) small SNRs.

with 32 blades, a magnetic exciter, three BTT probes, a once-per-revolution (OPR) reference sensor, a protection cover, a data acquisition device and the vibration analysis software. Three BTT probes were fixed around the bladed disk through the holes in the protection cover and the angle between two adjacent BTT probes is equal to 6 degrees. Key experimental parameters are listed in Table 3. The blade located nearest the OPR marker is numbered as the first blade and the left blades are clockwise numbered from 2 to 32. The three BTT probes are numbered as 1#, 2# and 3#.

TABLE 3. Experimental parameters.

| Parameters                   | Values      |
|------------------------------|-------------|
| Blade material               | 40 Cr steel |
| Blade length                 | 34 mm       |
| Blade width                  | 11 mm       |
| Blade tip thickness          | 3 mm        |
| Blade tip radius             | 69 mm       |
| Number of blades             | 32          |
| Number of BTT probes         | 3           |
| Number of OPR sensors        | 1           |
| Angle of adjacent BTT probes | 6°          |
| Variable rotating speed      | 0~20000 rpm |

It is difficult to generate cracks in the blades through rotation in the experiment, so different sizes of cracks are artificially cut at the roots of eight blades (15~22). The cracked blades are shown in Figure 16(b) and the depths of cracks are listed in Table 4. According to installation angles of the three BTT probe, the MCS pattern is represented as (60, 3, {0, 1, 2}). Here the 7<sup>th</sup> blade is selected as the normal blade. During the experiment, the rotating speed increases from 0 to 20000rpm, and the OPR & TOA signals are collected. Then angular-domain vibration displacements of each blade are calculated.

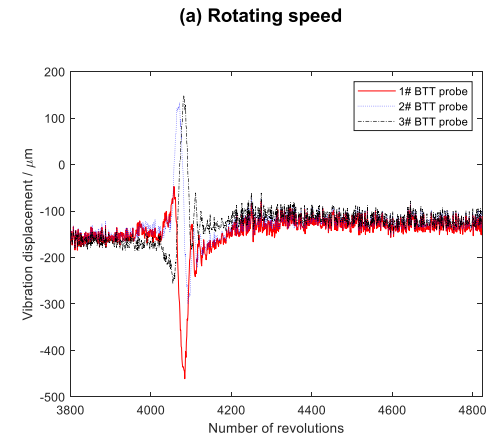
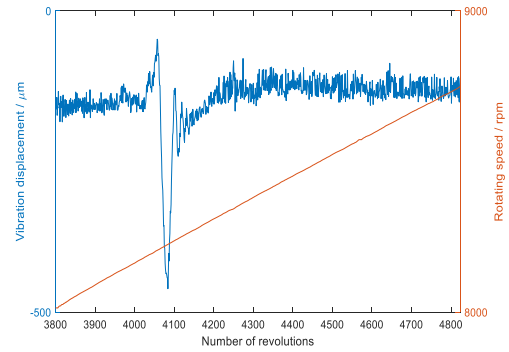
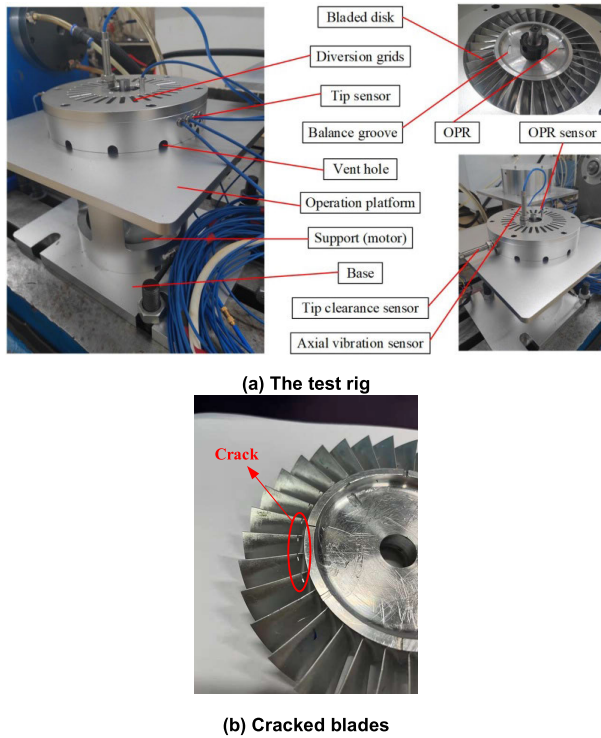


FIGURE 16. Experimental set-up.

TABLE 4. The crack depths in different blades.

| Number of blade | Crack depth | Number of blade | Crack depth |
|-----------------|-------------|-----------------|-------------|
| 15              | 0.3mm       | 19              | 1.5 mm      |
| 16              | 0.6 mm      | 20              | 1.8 mm      |
| 17              | 0.9 mm      | 21              | 2.1 mm      |
| 18              | 1.2 mm      | 22              | 3.0 mm      |

i) Firstly, angular-domain vibration displacements of 32 blades in the range of 7710~8731 rpm are recorded. Taking the 7<sup>th</sup> blade as an example, the rotating speed and vibration displacement from three BTT probes are measured and shown in Figure 17.

It can be seen that the vibration amplitude increases obviously near the 4100<sup>th</sup> revolution. By referring to the Campbell diagram of the blade, it can be understood that high-frequency resonant vibration occurs at this time and the vibration EO is equal to 15. As for the 7<sup>th</sup>, 17<sup>th</sup>, 18<sup>th</sup> and 20<sup>th</sup> blades, 400 groups of vibration displacements were chronologically collected for each blade and the length of each group is equal to 1024. Vibration displacements of the 7<sup>th</sup> blade are considered as the normal samples, and vibration displacements of the 17<sup>th</sup>, 18<sup>th</sup> and 20<sup>th</sup> blades are used for crack samples. Then 400 groups of normal samples are used to train the 4-layer VampNet model shown in Figure 3 and the learning rate

(b) Vibration displacements from three BTT probes

FIGURE 17. Measured rotating speed and vibration displacements of the 7<sup>th</sup> blade.

is set as 0.001. After that, the trained VampNet model is used to reconstruct the order spectrum of all normal samples and crack samples, respectively.

ii) The Campbell diagram of the cracked blade can be obtained in advance by using finite element simulations, which is shown in Figure 18. It can be seen that the rotating speed corresponding to the same vibration EO tends to decrease with the size of crack. That is to say, other vibration EOs may appear in the range of 7710~8731 rpm due to the crack. Based on it, the amplitudes at the 13<sup>th</sup>, 13.5<sup>th</sup>, 14<sup>th</sup> and 14.5<sup>th</sup> EOs in the reconstructed order spectrum are selected as the candidate monitored variables.

iii) Similarly, time series of all monitored variable are generated by using the normal samples and then the ADF test is carried out. The result shows that the amplitudes at the 13.5<sup>th</sup> and 14.5<sup>th</sup> EOs are cointegrating variables. Then the cointegrating vector is estimated as [-7532, 5514] by using the Johansen estimation. The cointegrating vector is used to calculate the cointegrating residuals of the normal samples (the 7<sup>th</sup> blade) and the crack samples (the 17<sup>th</sup>, 18<sup>th</sup> and 20<sup>th</sup> blades). The results are shown in Figure 19 and it can be seen that the cointegrating residuals of the crack samples obviously deviates from those of the normal samples. Also the deviation tends to increase with the size of crack.

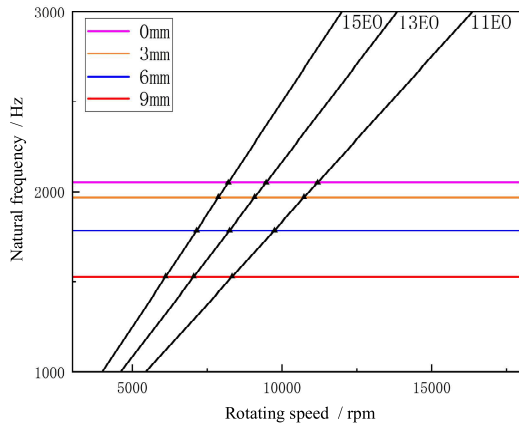


FIGURE 18. The Campbell diagram of the cracked blade.

In conclusion, 0.9mm crack can be effectively detected by using the cointegrating residual-based method.

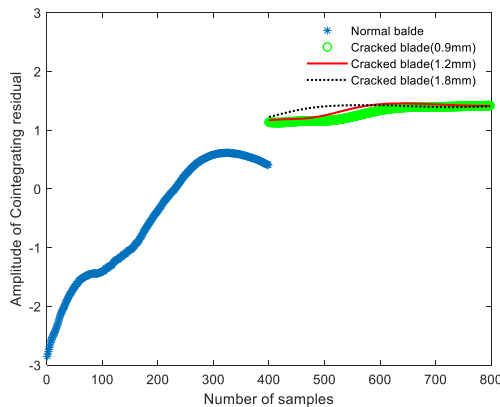


FIGURE 19. Experimental results of crack detection.

## VII. CONCLUSION

Due to under-sampling, it is very difficult to apply the BTT technique to detect blade damages under variable conditions. For this purpose, this paper proposes a VampNet-based learning reconstruction method of BTT vibration signals and then realizes cointegration-based blade damage detection. The following main conclusions can be drawn as follows.

(1) A discrete MCS-based CS model of BTT vibration signal is built in order domain to deal with variable rotating speeds, where an IHP window is integrated to reduce order spectrum leakage in discretization.

(2) The VampNet is introduced and built to achieve learning reconstruction of BTT vibration signal, which has simpler architecture, fewer super-parameters and better interpretability than classical DNNs.

(3) Based on reconstructed vibration EOs, cointegrating analysis is proposed for blade damage detection under variable conditions. In this case, the influences of variable conditions can be reduced.

(4) The superiority of the proposed method is testified by Matlab simulations and experimental results.

Frankly speaking, the proposed method in this paper has its own limitations. Firstly, how to determine the number of layers in VampNet is not discussed and it is also an open issue similar to that in classical DNNs. Secondly, the proposed method cannot be used to distinguish single damage from multiple damages due to the utilization of cointegrating residual. For this purpose, new damage detection methods deserve to be studied in future works. Thirdly, the proposed method also depends on training samples and the generalization ability is not discussed. In future works, we will further carry out other experiments to simulate different operation conditions and validate the proposed method.

In addition, combining CS with deep learning has become a future direction, where it is very promising to explore other potential DNN models and novel optimizers (e.g. meta-heuristic optimization techniques [31]) for BTT vibration reconstruction.

## ACKNOWLEDGMENT

The authors would like to thank the experimental set-up provided by Beijing Key Laboratory of Health Monitoring and Self-Recovery for High-End Mechanical Equipment, Beijing University of Chemical Technology.

## REFERENCES

- [1] P. Kaewniam, M. Cao, N. F. Alkayem, D. Li, and E. Manoach, "Recent advances in damage detection of wind turbine blades: A state-of-the-art review," *Renew. Sustain. Energy Rev.*, vol. 167, Oct. 2022, Art. no. 112723.
- [2] M. Civera and C. Surace, "An application of instantaneous spectral entropy for the condition monitoring of wind turbines," *Appl. Sci.*, vol. 12, no. 3, p. 1059, Jan. 2022.
- [3] A. Panagiotopoulos, T. Dmitri, and F. D. Spiliotis, "Damage detection on the blade of an operating wind turbine via a single vibration sensor and statistical time series methods: Exploring the performance limits of robust methods," *Structural Health Monitor.*, vol. 22, no. 1, pp. 433–448, May 2022.
- [4] M. Tiboni, C. Remino, R. Bussola, and C. Amici, "A review on vibration-based condition monitoring of rotating machinery," *Appl. Sci.*, vol. 12, no. 3, p. 972, Jan. 2022.
- [5] S. Heath and M. Imregun, "A survey of blade tip-timing measurement techniques for turbomachinery vibration," *J. Eng. Gas Turbines Power*, vol. 120, no. 4, pp. 784–791, Oct. 1998.
- [6] Z. Chen, H. Sheng, Y. Xia, W. Wang, and J. He, "A comprehensive review on blade tip timing-based health monitoring: Status and future," *Mech. Syst. Signal Process.*, vol. 149, Feb. 2021, Art. no. 107330.
- [7] J. R. Kadambi, R. D. Quinn, and M. L. Adams, "Turbomachinery blade vibration and dynamic stress measurements utilizing nonintrusive techniques," *J. Turbomachinery*, vol. 111, no. 4, pp. 468–474, Oct. 1989.
- [8] C. Lawson and P. Ivey, "Tubomachinery blade vibration amplitude measurement through tip timing with capacitance tip clearance probes," *Sens. Actuators A, Phys.*, vol. 118, no. 1, pp. 14–24, Jan. 2005.
- [9] B. Salhi, J. Lardies, and M. Berthillier, "Identification of modal parameters and aeroelastic coefficients in bladed disk assemblies," *Mech. Syst. Signal Process.*, vol. 23, no. 6, pp. 1894–1908, Aug. 2009.
- [10] Z. Chen, Y. Yang, Y. Xie, B. Guo, and Z. Hu, "Non-contact crack detection of high-speed blades based on principal component analysis and Euclidian angles using optical-fiber sensors," *Sens. Actuators A, Phys.*, vol. 201, pp. 66–72, Oct. 2013.
- [11] S. Chen, Y. Yang, H. Hu, F. Guan, G. Shen, Z. Bian, and H. Guo, "Interpolation method for wideband signal reconstruction based on blade tip timing measurement," *Measurement*, vol. 176, May 2021, Art. no. 109168.

- [12] J. Cao, Z. Yang, S. Tian, and X. Chen, "Time delay-based spectrum reconstruction for nonuniform and sub-nyquist sampling in blade tip timing," *Mech. Syst. Signal Process.*, vol. 200, Oct. 2023, Art. no. 110552.
- [13] J. Lin, Z. Hu, Z.-S. Chen, Y.-M. Yang, and H.-L. Xu, "Sparse reconstruction of blade tip-timing signals for multi-mode blade vibration monitoring," *Mech. Syst. Signal Process.*, vol. 81, pp. 250–258, Dec. 2016.
- [14] J. Tian, X. Zhang, Y. Chen, P. Russhard, and H. Ouyang, "Sparse reconstruction method of non-uniform sampling and its application in blade tip timing system," in *Proc. Struct. Dyn., Struct. Mech., Vibrat., Damping; Supercritical CO<sub>2</sub>*, vol. 11, Sep. 2020, Paper GT2020-14753.
- [15] D. L. Donoho, "Compressed sensing," *IEEE Trans. Inf. Theory*, vol. 52, no. 4, pp. 1289–1306, Apr. 2006.
- [16] H. L. Xu, Z. S. Chen, Y. M. Yang, and L. M. Tao, "Multi-band blade vibration monitoring by blade tip-timing method based on compress sensing," in *Proc. 1st World Congr. Condition Monit.*, London, U.K., Jun. 2017, pp. 481–491.
- [17] M. Pan, Y. Yang, F. Guan, H. Hu, and H. Xu, "Sparse representation based frequency detection and uncertainty reduction in blade tip timing measurement for multi-mode blade vibration monitoring," *Sensors*, vol. 17, no. 8, p. 1745, Jul. 2017.
- [18] R. P. Spada and R. Nicoletti, "Applying compressed sensing to blade tip timing data: A parametric analysis," in *Proc. 10th Int. Conf. Rotor Dyn.* Cham, Switzerland: Springer, 2018, pp. 121–134.
- [19] Z. Liu, F. Duan, G. Niu, D. Ye, J. Feng, Z. Cheng, X. Fu, J. Jiang, J. Zhu, and M. Liu, "Reconstruction of blade tip-timing signals based on the MUSIC algorithm," *Mech. Syst. Signal Process.*, vol. 163, Jan. 2022, Art. no. 108137.
- [20] D. L. Donoho and J. Tanner, "Precise undersampling theorems," *Proc. IEEE*, vol. 98, no. 6, pp. 913–924, Jun. 2010.
- [21] Z. Chen, H. Sheng, and Y. Xia, "Multi-coset angular sampling-based compressed sensing of blade tip-timing vibration signals under variable speeds," *Chin. J. Aeronaut.*, vol. 34, no. 9, pp. 83–93, Sep. 2021.
- [22] J. C. Ye, Y. Han, and E. Cha, "Deep convolutional framelets: A general deep learning framework for inverse problems," *SIAM J. Imag. Sci.*, vol. 11, no. 2, pp. 991–1048, Jan. 2018.
- [23] Z. Chen, H. Sheng, L. Liao, C. Liu, and Y. Xiong, "Deep learning for compressed sensing-based blade vibration reconstruction from sub-sampled tip-timing signals," *IEEE Access*, vol. 11, pp. 38251–38262, 2023.
- [24] D. L. Donoho, A. Maleki, and A. Montanari, "Message passing algorithms for compressed sensing," *Proc. Nat. Acad. Sci. USA*, vol. 106, no. 45, pp. 18914–18919, Nov. 2009.
- [25] S. Rangan, P. Schniter, and A. K. Fletcher, "Vector approximate message passing," 2016, *arXiv:1610.03082*.
- [26] M. Borgerding, P. Schniter, and S. Rangan, "AMP-inspired deep networks for sparse linear inverse problems," 2016, *arXiv:1612.01183*.
- [27] P. Depalle and T. Helie, "Extraction of spectral peak parameters using a short-time Fourier transform modeling and no sidelobe windows," in *Proc. Workshop Appl. Signal Process. Audio Acoust.*, Oct. 1997, p. 4.
- [28] R. F. Engle and C. W. J. Granger, "Co-integration and error correction: Representation, estimation, and testing," *Econometrica*, vol. 55, no. 2, p. 251, Mar. 1987.
- [29] E. J. Cross, G. Manson, K. Worden, and S. G. Pierce, "Features for damage detection with insensitivity to environmental and operational variations," *Proc. Roy. Soc. A, Math., Phys. Eng. Sci.*, vol. 468, no. 2148, pp. 4098–4122, Dec. 2012.
- [30] H. Xu, Z. Chen, Y. Xiong, Y. Yang, and L. Tao, "Nonlinear dynamic behaviors of rotated blades with small breathing cracks based on vibration power flow analysis," *Shock Vibrat.*, vol. 2016, pp. 1–11, Aug. 2016.
- [31] V. Tomar, M. Bansal, and P. Singh, "Metaheuristic algorithms for optimization: A brief review," *Eng. Proc.*, vol. 59, Mar. 2023, Art. no. 238.

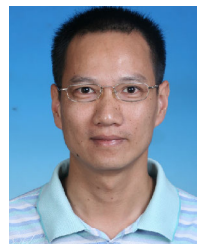


**ZHONGSHENG CHEN** (Member, IEEE) was born in Anhui, China, in 1977. He received the B.S., M.S., and Ph.D. degrees in mechanical engineering from the National University of Defense Technology, Changsha, China, in 1999, 2001, and 2004, respectively.

From 2004 to 2017, he was a Lecturer and an Associate Professor with the College of Mechatronic Engineering and Automation, National University of Defense Technology. From 2017 to 2022, he was a Professor with the College of Electrical and Information Engineering, Hunan University of Technology. Since July 2022, he has been a Professor with the College of Automotive Engineering, Changzhou Institute of Technology. His current research interests include fault diagnosis and prognostics, machine vision, and nonlinear vibration energy harvesting.



**HAOPENG LIU** was born in Hunan, China, in 1996. He received the B.S. degree from Hunan University of Technology, in 2021, where he is currently pursuing the master's degree. His research interest includes BTT-based vibration monitoring.



**LIANYING LIAO** was born in Fujian, China, in 1978. He received the B.S. and M.S. degrees in vehicle engineering from Wuhan University of Technology, Wuhan, China, in 2001 and 2004, respectively, and the Ph.D. degree in vehicle engineering from Jiangsu University, Zhenjiang, China, in 2018.

From 2004 to 2023, he was a Lecturer, an Associate Professor, and a Professor with the College of Automotive Engineering, Changzhou Institute of Technology. His current research interests include embedded fault diagnosis and prognostics, noise, and vibration reduction technology for vehicles.

• • •